Journal of ELECTRONIC MATERIALS, Vol. 43, No. 11, 2014
DOI: 10.1007/s11664-014-3323-y


# Mechanical Deformation Behavior of Sn-Ag-Cu Solders with Minor Addition of 0.05 wt.% Ni

A.E. HAMMAD[1,2,3] and A.M. EL-TAHER[1]

1.—Physics Department, Faculty of Science, Zagazig University, Zagazig, Egypt. 2.—e-mail: a_hammad_82@yahoo.com. 3.—e-mail: a_hammad@zu.edu.eg

The aim of the present work is to develop a comparative evaluation of the microstructural and mechanical deformation behavior of Sn-Ag-Cu (SAC) solders with the minor addition of 0.05 wt.% Ni. Test results showed that, by adding 0.05Ni element into SAC solders, generated mainly small rod-shaped $(Cu,Ni)_6Sn_5$ intermetallic compounds (IMCs) inside the $\beta$-Sn phase. Moreover, increasing the Ag content and adding Ni could result in the change of the shape and size of the IMC precipitate. Hence, a significant improvement is observed in the mechanical properties of SAC solders with increasing Ag content and Ni addition. On the other hand, the tensile results of Ni-doped SAC solders showed that both the yield stress and ultimate tensile strengths decrease with increasing temperature and with decreasing strain rate. This behavior was attributed to the competing effects of work hardening and dynamic recovery processes. The Sn-2.0Ag-0.5Cu-0.05Ni solder displayed the highest mechanical properties due to the formation of hard $(Cu,Ni)_6Sn_5$ IMCs. Based on the obtained stress exponents and activation energies, it is suggested that the dominant deformation mechanism in SAC (205)-, SAC (0505)- and SAC (0505)-0.05Ni solders is pipe diffusion, and lattice self-diffusion in SAC (205)-0.05Ni solder. In view of these results, the Sn-2.0Ag-0.5Cu-0.05Ni alloy is a more reliable solder alloy with improved properties compared with other solder alloys tested in the present work.

**Key words:** Lead-free solders, Sn-Ag-Cu alloy, microstructure, mechanical properties

## INTRODUCTION

In recent years, the increasing demand for portable electronics has led to the shrinking in size of electronic components and solder joint dimensions.[1] Furthermore, driven by government legislation, the electronics industry has advanced to lead-free solders due to environmental and health concerns emanating from the use of Pb-based solders.[2–5] To date, several types of lead-free solders have been developed such as Sn-Ag, Sn-Cu, Sn-Bi and Sn-Ag-Cu alloys.[6,7] Sn-Ag-Cu (SAC) alloy has good mechanical properties and wettability, making it the most widely used lead-free solder.[8,9] However, according to the literature,[10,11] SAC solder alloys with high Ag content are more brittle in nature than Sn-Pb solders due to the intermetallic compounds (IMC) $Cu_6Sn_5$ and $Cu_3Sn$ formed at the SAC solder/Cu interface; $Ag_3Sn$ IMC formed at the SAC solder/Ag interface. In addition, the high Ag content increases the relative cost for the products. Thus, it is almost mandatory to shift to low-Ag-content SAC alloys. Reducing the Ag content can improve the reliability of SAC solder joints in dynamic environments.[12] It has been proved that, to further enhance the properties of SAC solder alloys, alloying elements such as Bi, Ni, P and Ce have been added to these alloys.[13–15] Among them, the Ni element is usually an effective additive because adding the Ni element cannot improve the wettability and anti-oxidization of the Sn-3.0Ag-0.5Cu (SAC305) solder alloy, but it can depress the interfacial IMC growth due to the high temperature aging and it then

(Received March 24, 2014; accepted July 5, 2014; published online July 26, 2014)

improves the shear strength of the solder joint.[15] In previous studies, Ni additives had little effect on the tensile strength of SAC (305) solder, but obviously suppressed the elongation ratio and reduction of area.[16] In light of the above, the aim of this study is to develop a comparative evaluation of the microstructural and mechanical properties of as-cast SAC (205) and SAC (0505) solders containing 0.05Ni.

## EXPERIMENTAL PROCEDURE AND DESIGN

Pure tin (99.999%), silver (99.9%), copper (99.99%), and nickel (99.999%) were used as raw materials and melted in a vacuum furnace under high-purity argon atmosphere. Then, the ingots were homogenized at 500 ± 4°C for 3600 s to produce solder alloys of Sn-2.0Ag-0.5Cu [SAC (205)], Sn-0.5Ag-0.5Cu [SAC (0505)], Sn-2.0Ag-0.5Cu-0.05Ni [SAC (205)-0.05Ni] and Sn-0.5Ag-0.5Cu-0.05Ni [SAC (0505)-0.05Ni] (all in wt.%). The chemical compositions of the solder alloys are shown in Table I. The molten solder for each sample in the crucible was chill-cast in a copper mold to form cylindrical ingots of 10 mm diameter. A cooling rate of 6–8°C/s was achieved so as to create the fine microstructure typically found in small solder joints in microelectronic packages. The solder ingots were then mechanically machined into wire samples with a gauge length of $4.0 \times 10^{-2}$ m and $2.5 \times 10^{-3}$ m in diameter, as developed in our previous work.[17] All the ingots were heat-treated at 130°C for 1800 s before being machined to tensile specimens.

The microstructures were observed using a scanning electron microscope (SEM) after all the

**Table I. Chemical composition of the studied solders (wt.%)**

| Alloy | Ag | Cu | Ni | Pb | Bi | Sb | As | Sn |
|---|---|---|---|---|---|---|---|---|
| Sn-2.0Ag-0.5Cu | 2.0 | 0.5 | – | 0.0061 | 0.0071 | 0.0042 | 0.0001 | Bal. |
| Sn-0.5Ag-0.5Cu | 0.5 | 0.5 | – | 0.0067 | 0.0066 | 0.0040 | 0.0001 | Bal. |
| Sn-2.0Ag-0.5Cu-0.05Ni | 2.0 | 0.5 | 0.05 | 0.0062 | 0.0072 | 0.0044 | 0.0001 | Bal. |
| Sn-0.5Ag-0.5Cu-0.05Ni | 0.5 | 0.5 | 0.05 | 0.0062 | 0.0067 | 0.0044 | 0.0001 | Bal. |

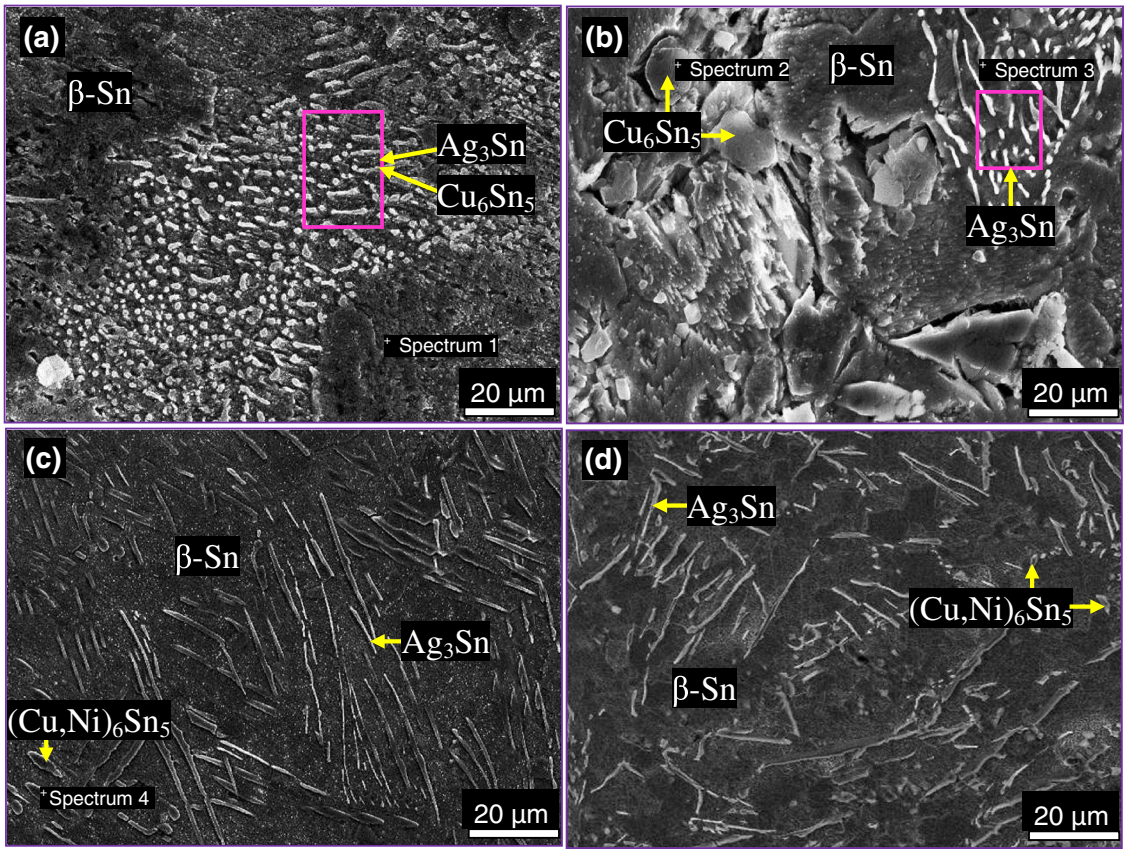


Fig. 1. SEM images of as-cast: (a) SAC (205), (b) SAC (0505), (c) SAC (205)-0.05Ni, and (d) SAC (0505)-0.05Ni solder alloys.

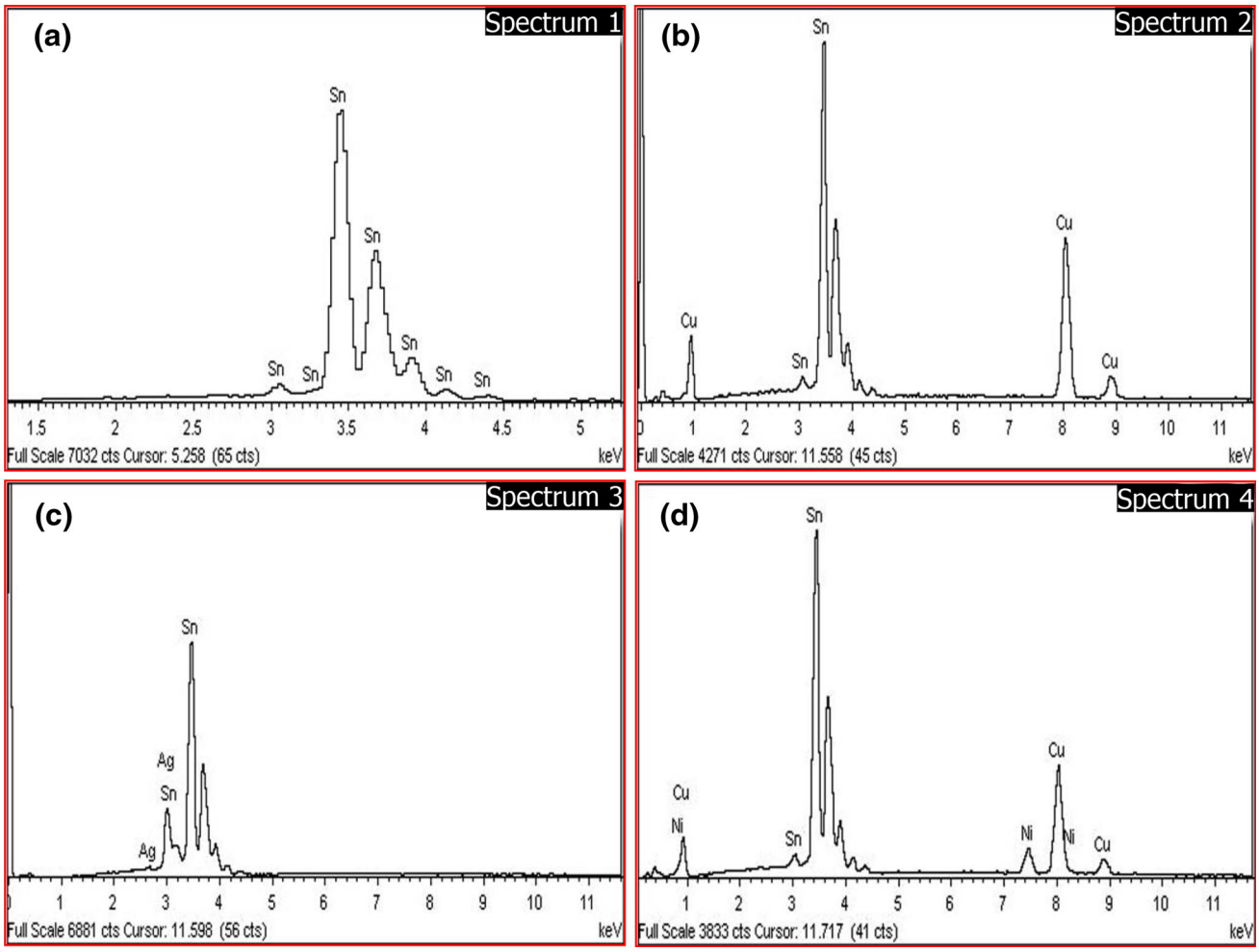


Fig. 2. EDS analysis result of (a) Sn, (b) $Cu_6Sn_5$, (c) $Ag_3Sn$ and (d) $(Cu,Ni)_6Sn_5$ IMC particles in the selected solder.

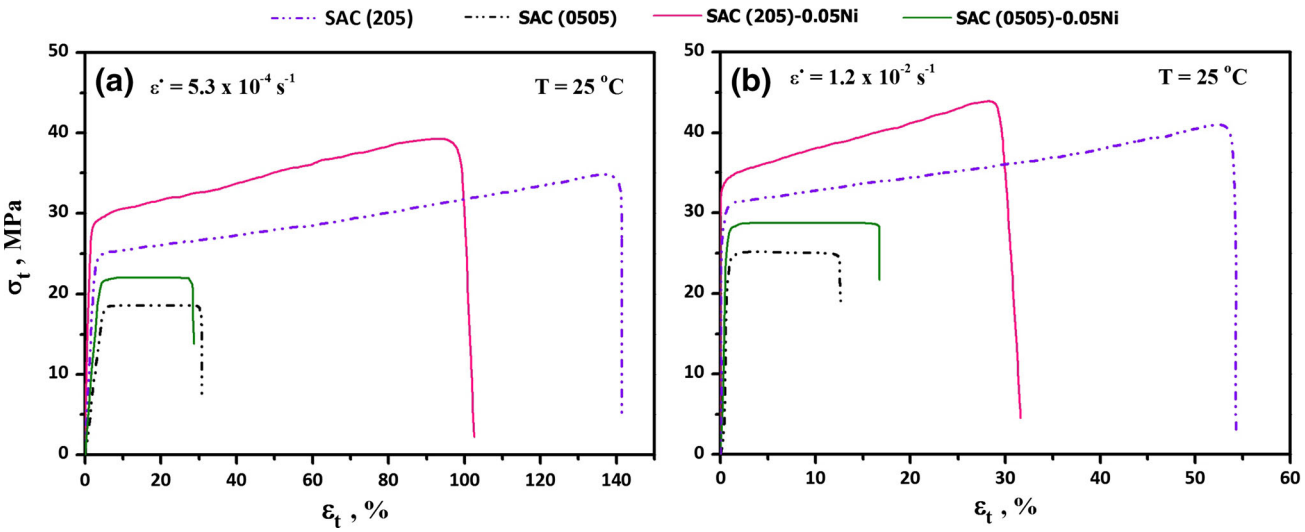


Fig. 3. Comparative tensile stress–strain curves for SAC (205), SAC (0505), SAC (205)-0.05Ni and SAC (0505)-0.05Ni alloys, obtained at room temperature and strain rates: (a) $\dot{\varepsilon} = 5.3 \times 10^{-4}\ s^{-1}$ and (b) $\dot{\varepsilon} = 1.2 \times 10^{-2}\ s^{-1}$.

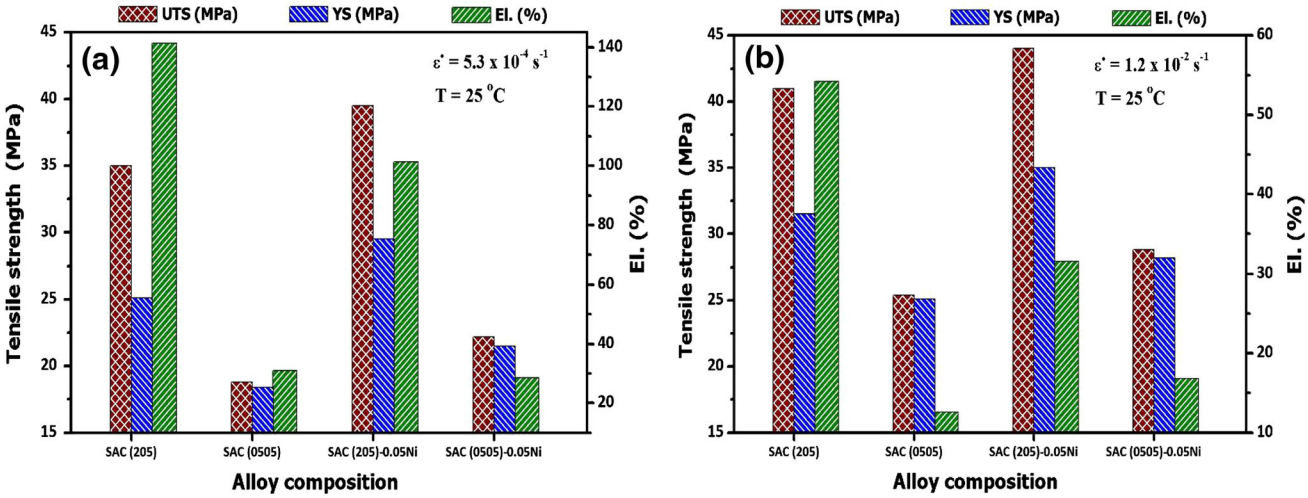


Fig. 4. Mechanical properties: tensile strength and elongation of the samples at $T = 25°C$ and strain rates: (a) $\dot{\varepsilon} = 5.3 \times 10^{-4}\ s^{-1}$ and (b) $\dot{\varepsilon} = 1.2 \times 10^{-2}\ s^{-1}$.

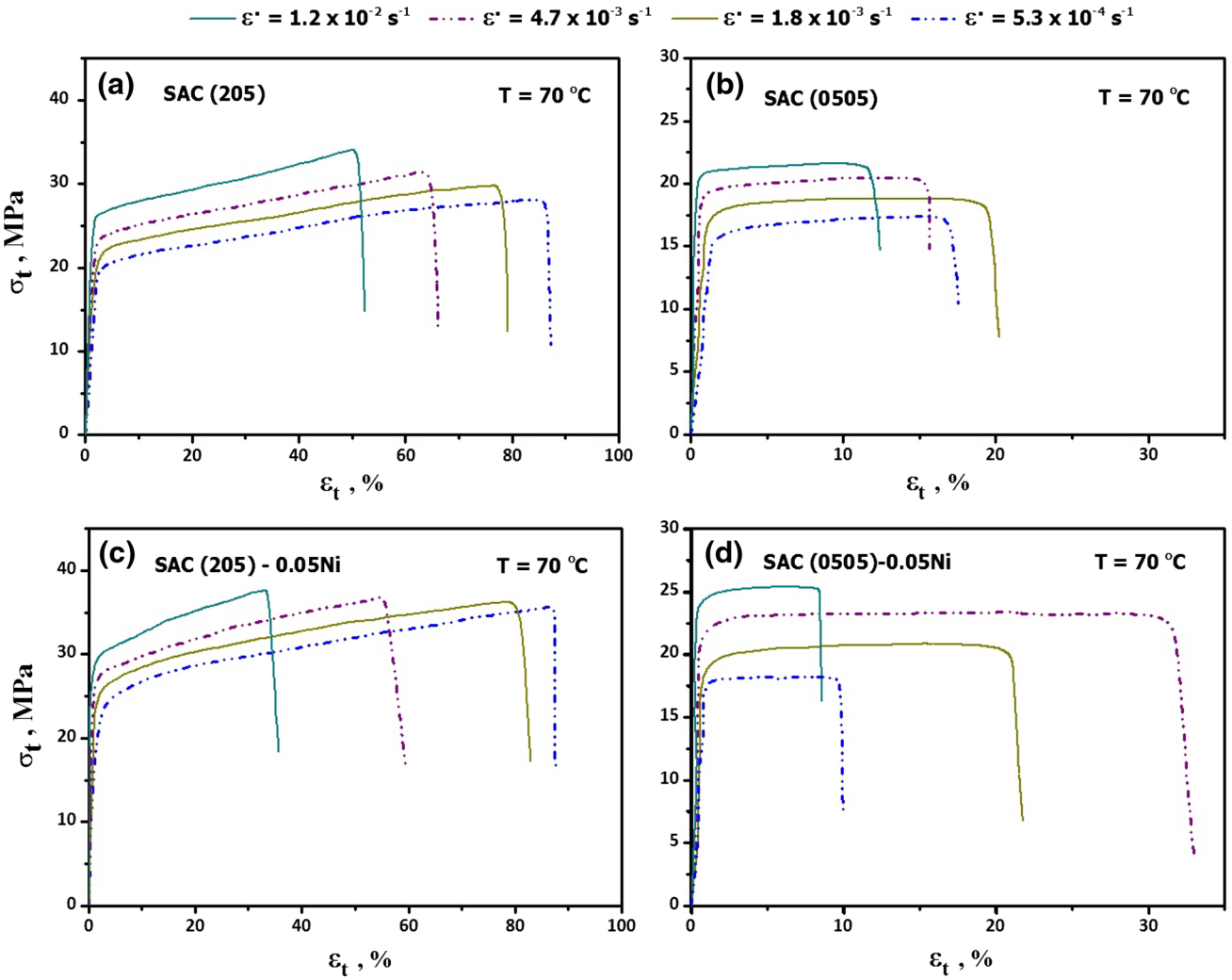


Fig. 5. Stress–strain curves of: (a) SAC (205), (b) SAC (0505), (c) SAC (205)-0.05Ni and (d) SAC (0505)-0.05Ni alloys, obtained at 70°C and different strain rates.

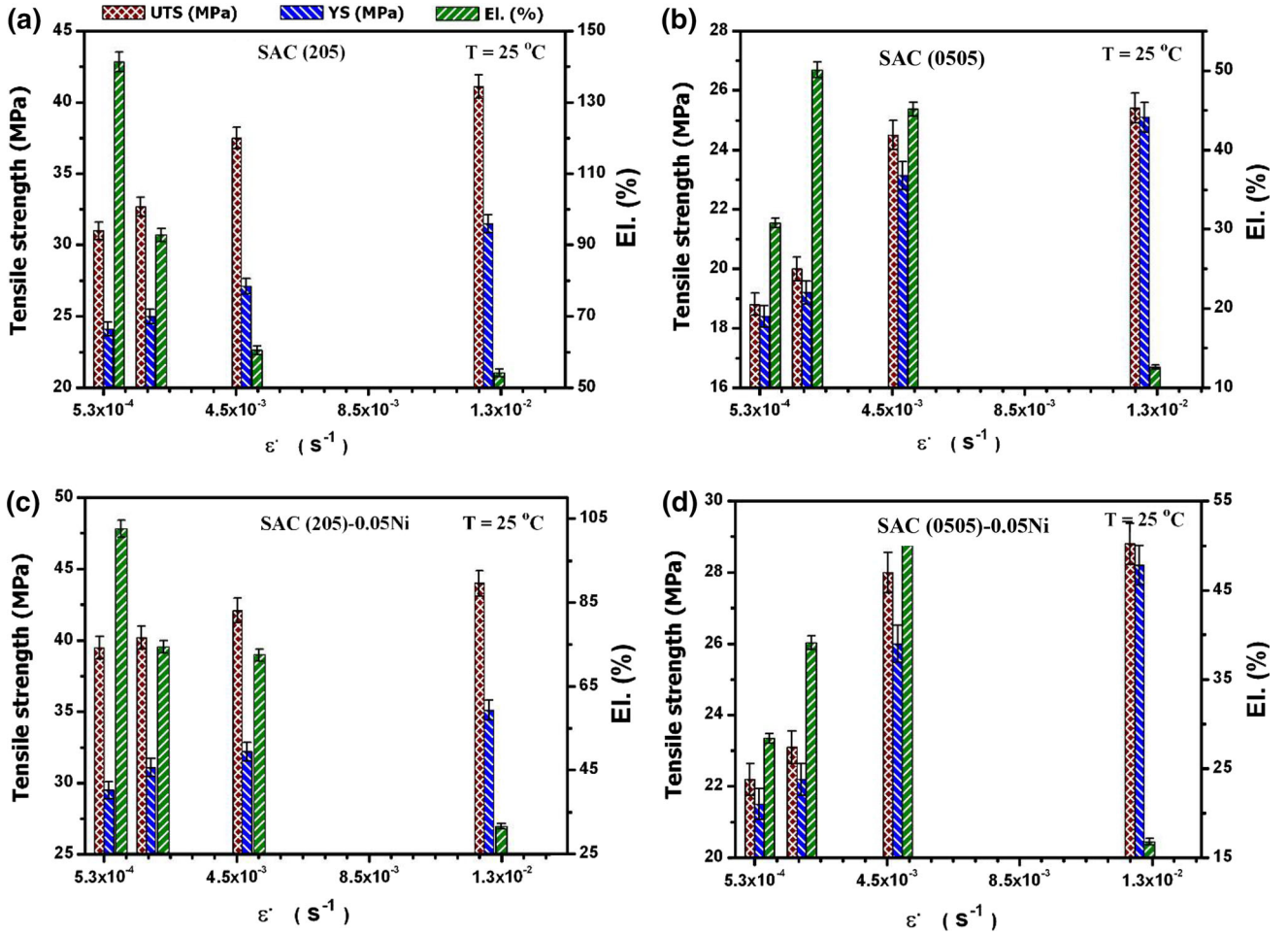


Fig. 6. Tensile properties (UTS, YS and El.%) at $T$ = 25°C for (a) SAC (205), (b) SAC (0505), (c) SAC (205)-0.05Ni and (d) SAC (0505)-0.05Ni alloys.

samples were ground, polished and etched with a solution of 5 vol.% $HNO_3$–2 vol.%HCl-93 vol.% $CH_3OH$ for several seconds. The SEM used in this study was a JEOL model JSM-5410, Japan. The compositions of the IMC phases were identified using energy dispersive spectrometry (EDS).

The tensile tests were carried out using an Instron 3360 universal testing machine at constant strain rate and different temperatures ranging from 25°C to 110°C. The tests were also performed at constant temperatures 25°C, 70°C and 110°C and various strain rates ranging from $10^{-4}$ $s^{-1}$ to $10^{-2}$ $s^{-1}$. For each specimen, six tests were performed and average was taken. The environment chamber temperature could be monitored by using a thermocouple contacting with specimen.

## RESULTS AND DISCUSSION

### Microstructural Investigation

To clearly identify the microstructure of the selected alloys, SEM together with the EDS analyses of the constituent phases were used. Figure 1 shows as-cast microstructures of the SAC (205), SAC (0505), SAC (205)-0.05Ni and SAC (0505)-0.05Ni solders. In Fig. 1a and b, the microstructure of SAC (205) and SAC (0505) consist of eutectic regions of IMCs dispersed within a Sn-rich matrix. Using EDS compositional analysis, the black area is identified as Sn (Fig. 2a), and the IMC particles are identified as $Cu_6Sn_5$ (Fig. 2b) and $Ag_3Sn$ (Fig. 2c). The $Ag_3Sn$ and $Cu_6Sn_5$ phases are well known to have the highest strength among the constituent phases in SAC alloys, whereas the primary $\beta$-Sn phase has the lowest elastic modulus and yield strength in SAC alloys.[18] It is observed in Fig. 1a and c that high Ag-content in SAC solders increases the amount of IMCs precipitates and decreases the fraction of the Sn matrix compared with the low Ag-content solders shown in Fig. 1b and d. This result is consistent with a previous study.[11] Accordingly, it is expected that SAC (205)-0.05Ni solder shows the highest mechanical properties and fatigue resistance because of precipitate strengthening.[19]

Adding 0.05Ni element into SAC solders generated mainly small rod-shaped IMCs inside the $\beta$-Sn

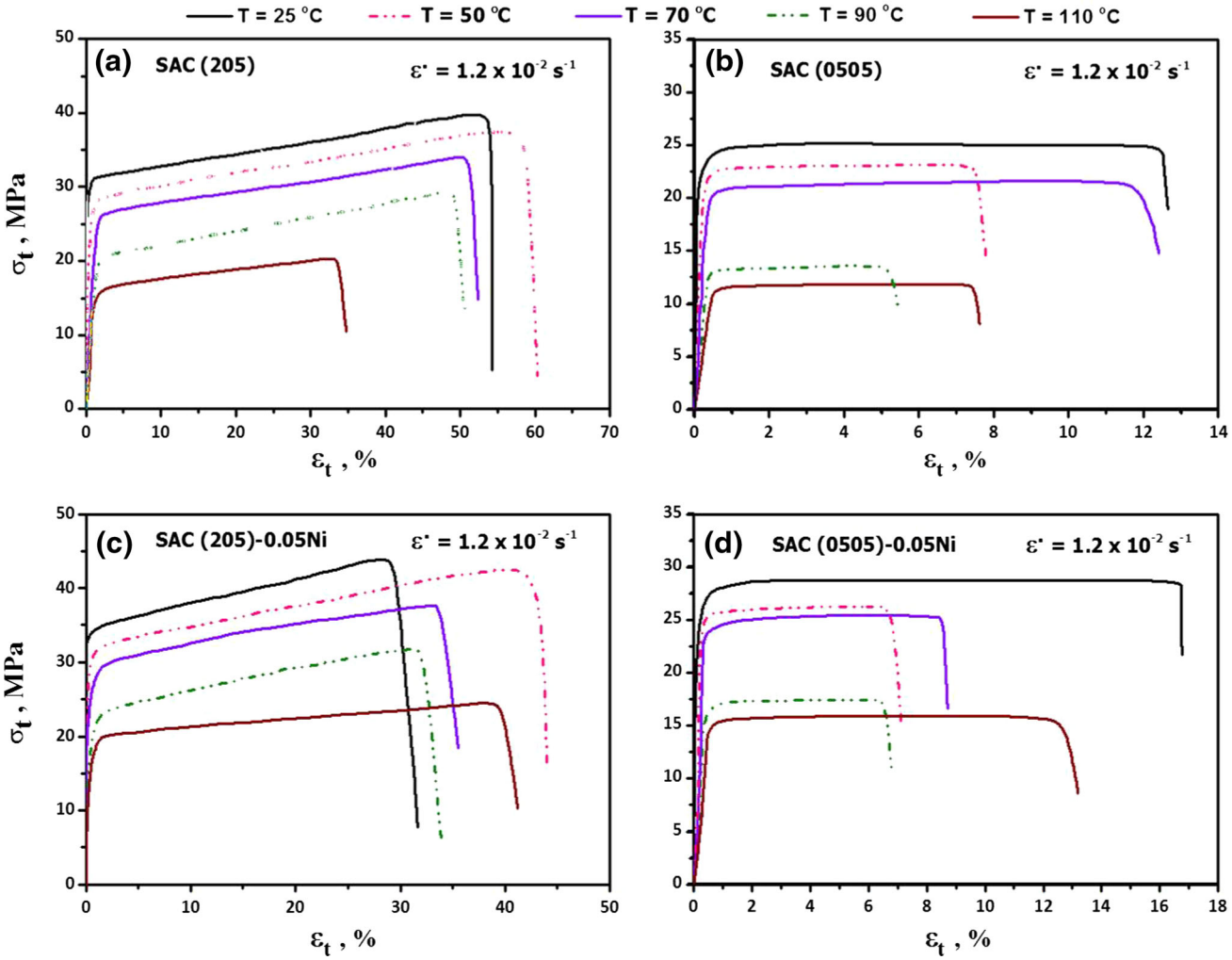


Fig. 7. Stress–strain plots at constant strain rate of 1.2 × $10^{-2}$ $s^{-1}$ and different temperatures for (a) SAC (205), (b) SAC (0505), (c) SAC (205)-0.05Ni and (d) SAC (0505)-0.05Ni alloys.

phase, as illustrated in Fig. 1c and d. The results of EDS analysis indicated that these IMCs are $(Cu,Ni)_6Sn_5$, as shown in Fig. 2d. This implied that the Ni atoms could promote the formation of $(Cu,Ni)_6Sn_5$ IMC and replace some fraction of Cu atoms in the Cu-Sn IMCs. As we know, the standard Gibbs energy of formation of Cu-Sn is lower than that of Ni-Sn. In addition, the solubility of Ni could significantly stabilize $(Cu,Ni)_6Sn_5$.[16] Because the solubility of Ni is zero in the $\beta$-Sn phase and very high in the $Cu_6Sn_5$ phase,[20] Ni, like Cu, is transferred from $\beta$-Sn to the IMC phase during coupled growth. This suggests that Ni addition may significantly decline $Ni_3Sn_4$ formation in Sn-rich SAC alloys. As both $(Cu,Ni)_6Sn_5$ and $Ni_3Sn_4$ grew as primary phases in the same sample, and both were present at the onset of the eutectic reaction, the presence of $(Cu,Ni)_6Sn_5$ does not seem to be related to nucleation difficulties of $Ni_3Sn_4$. Instead, the increasing ratio of primary $(Cu,Ni)_6Sn_5$ to primary $Ni_3Sn_4$ due to the high cooling rate suggests that $(Cu,Ni)_6Sn_5$ has easier growth kinetics than $Ni_3Sn_4$. Jiang et al.[21] reported that the addition of 0.1 wt.% Ni to Sn-1Ag-0.8Cu (SAC108) solder on an Ni/Au surface finish had no significant effect on the IMC layer growth. The addition of Ni to the SAC108 solders on an OSP surface finish hindered the formation of $Cu_3Sn$ but caused excessive $Cu_6Sn_5$ growth after solid-state aging.

Moreover, with increasing Ag content and 0.05 wt.% Ni addition in SAC solders, the as-cast microstructure is more uniform and much finer. In addition, the solubility of Ni can significantly stabilize $(Cu,Ni)_6Sn_5$.[16] Furthermore, the microstructure of the SAC (205)-0.05Ni solder exhibits $(Cu,Ni)_6Sn_5$ intermetallic strengthening phases, as shown in Fig. 1c. Therefore, it is expected to improve the strength of the solder. This result is consistent with previous works.[15,16]

## Mechanical Properties

Figure 3 shows the comparative stress versus strain curves of the as-cast SAC (205), SAC (0505), SAC (205)-0.05Ni and SAC (0505)-0.05Ni solder

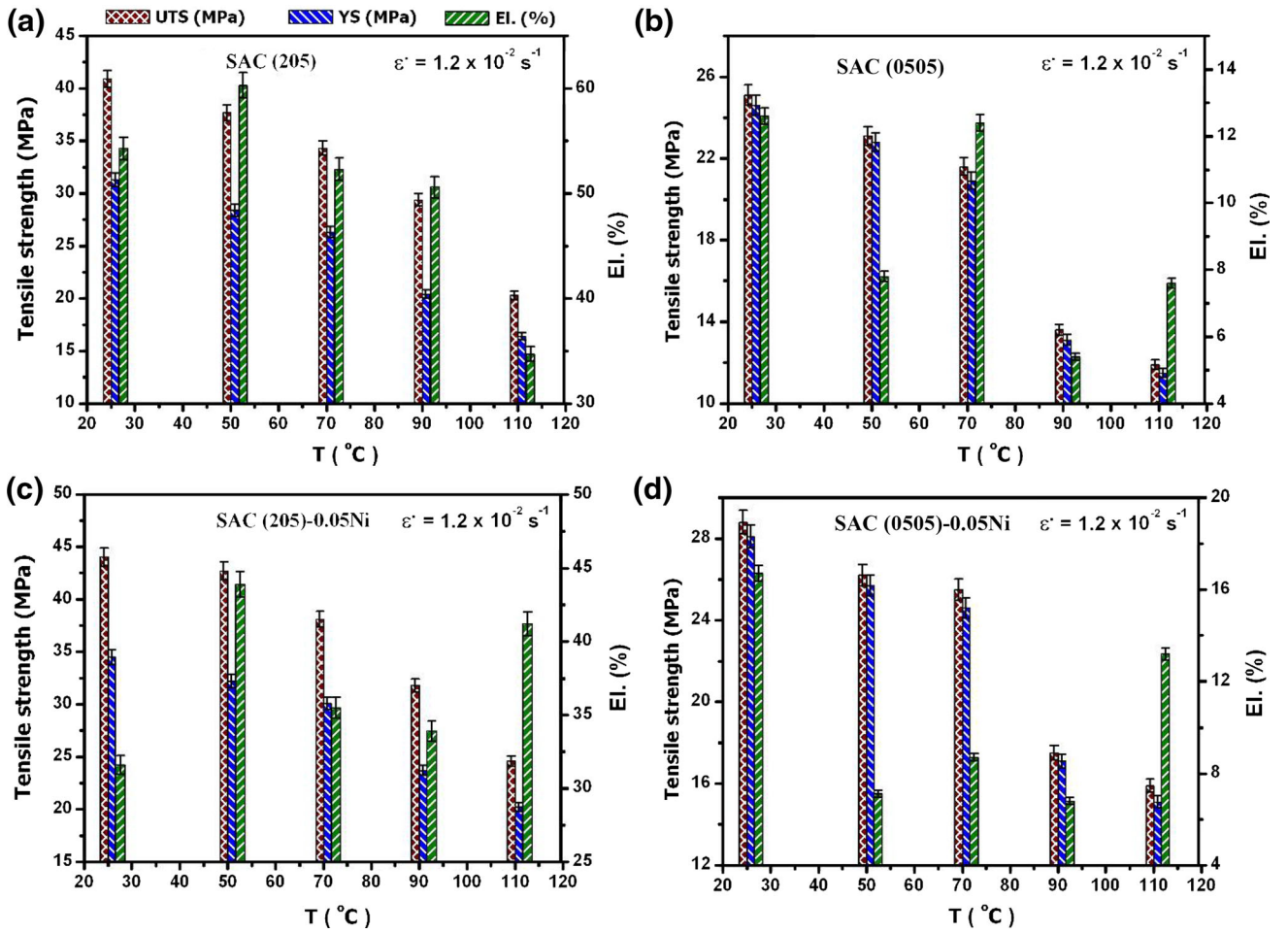


Fig. 8. Tensile properties (UTS, YS and El. %) at $\dot{\varepsilon} = 1.2 \times 10^{-2}\ s^{-1}$ for (a) SAC (205), (b) SAC (0505), (c) SAC (205)-0.05Ni and (d) SAC (0505)-0.05Ni alloys.

alloys at room temperature and strain rates of $5.3 \times 10^{-4}\ s^{-1}$ and $1.2 \times 10^{-2}\ s^{-1}$. As illustrated, both Ag content and Ni addition significantly affect the mechanical properties. It is well known that the nature of the stress–strain plots is a reflection of the relative dominance of work hardening and dynamic recovery processes during the deformation. For SAC (205) and SAC (205)-0.05Ni, the work hardening is more dominant than dynamic recovery processes. Such behavior can be understood by considering the deformation as a dispersion hardening mechanism of IMC phases in these alloys. These results are consistent with those of other studies.[22] However, during strain hardening, the dislocation density increases with intensifying the deformation, leading to further hindering of the dislocation movement. As a result, the imposed stress necessary to deform the material could increase with increasing strain hardening, leading to significant improvement in tensile strength in these alloys. For SAC (0505) and SAC (0505)-0.05Ni solders, the results show that an initial elastic region followed by a viscoplastic plateau, which results from the balancing of two antagonist mechanisms: work hardening and dislocations unpinning.[23] Such behavior has to be referred to the fact that at room temperature these alloys work in creep conditions, since room temperature exceeds half the absolute melting temperature of the solder alloys.

Figure 4a and b shows the average values of mechanical properties [i.e., 0.2% yield stress (YS), ultimate tensile strength (UTS), and total elongation (El. %)] of the tested solder alloys. The SAC (205) solder had UTS of 35.0, YS of 25.1 MPa, and El. of 141.3% higher than UTS of 18.8, YS of 18.4 MPa and El. of 31.0% of the SAC (0505) alloy at $\dot{\varepsilon} = 5.3 \times 10^{-4}\ s^{-1}$ and room temperature (Fig. 4a). A significant improvement in the tensile strength and elongation at failure are observed with increasing Ag content. Furthermore, adding 0.05 wt.% Ni results in an increase in YS and UTS due to the formation of $(Cu,Ni)_6Sn_5$ IMCs.

## Influence of Strain Rate on the Mechanical Properties

Tensile stress–strain curves at constant temperature of 70°C and various strain rates in the range $10^{-4}$–$10^{-2}\ s^{-1}$ are shown in Fig. 5. Irrespective of

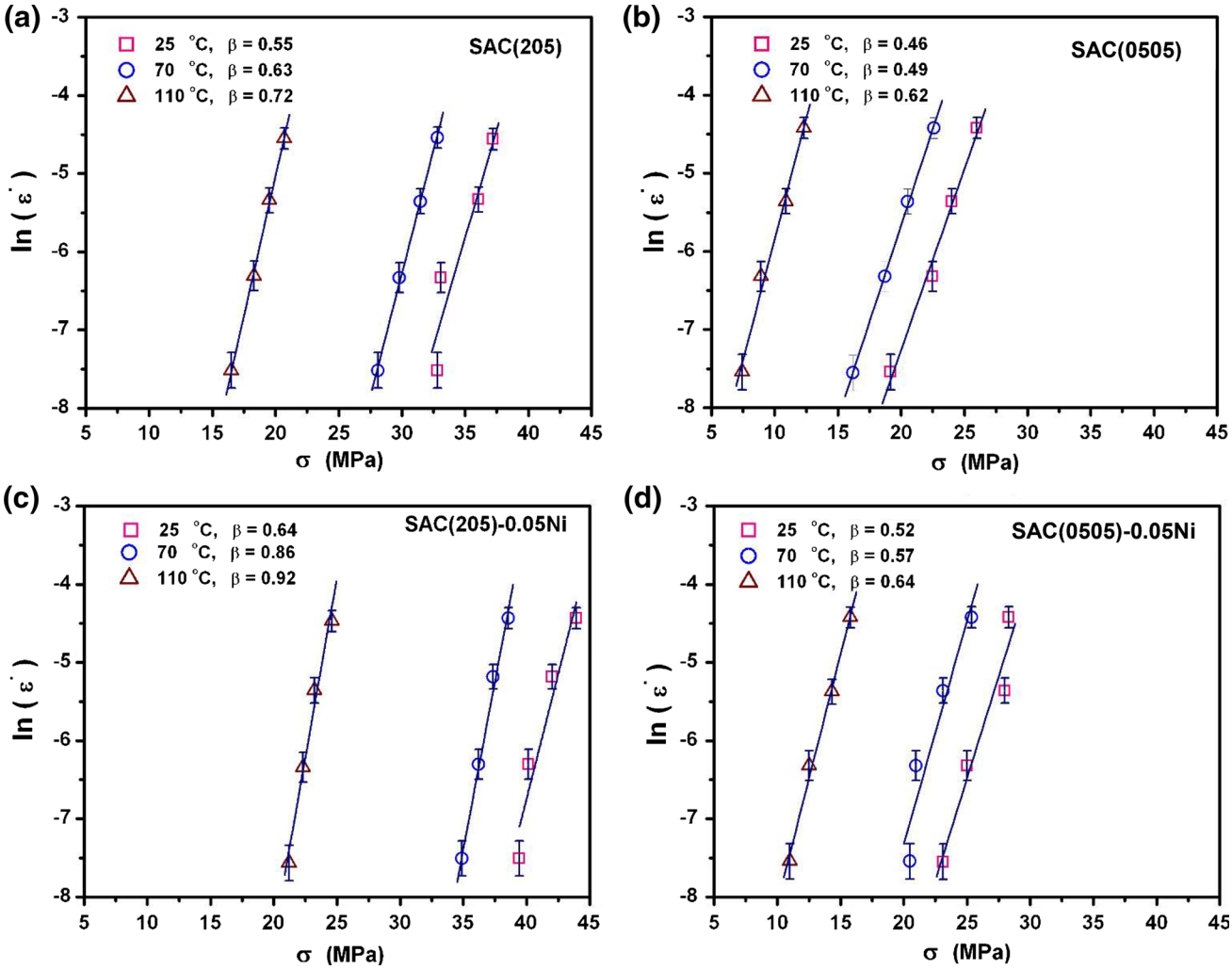


Fig. 9. The relationship between ln ($\dot{\varepsilon}$) versus $\sigma$ at $T$ = 25°C, 70°C and 110°C for (a) SAC (205), (b) SAC (0505), (c) SAC (205)-0.05Ni and (d) SAC (0505)-0.05Ni solder alloys.

the material type, it can be observed that the overall level of the stress–strain curves increases as the strain rate increases. To have a more complete view of the influence of the strain rate on the UTS, YS and El.% under all testing conditions, these three parameters were plotted against strain rates at constant temperature for different solders, as shown in Fig. 6. All alloys show the similar trend with strain rate effect that the UTS and YS increases as the deformation rate increases. These results indicate that the tensile behavior of the tested alloys often exhibits strong strain rate dependency and strain rate sensitivity.[24] The increase in tensile strength with strain rate can be explained by dislocations multiplication and dislocation–dislocation interaction. In solder alloys, the plastic flow is related directly to the presence, and response to an applied stress, of certain crystallographic defects called dislocations. When the solder is applied to stresses, the dislocations slip on the slip plane to resist the deformation.[25] The SAC (205)-0.05Ni alloy exhibits the highest tensile strength over the strain rate range. This can be attributed to the formation of $(Cu,Ni)_6Sn_5$ IMCs in the solder matrix and the refinement of $\beta$-Sn matrix as well as the sizes of the IMC particles. The variation of elongation with the strain rate comes from the interaction between IMCs or precipitates with the dislocation motion.[19]

## Influence of temperature on the mechanical properties

Figure 7 shows the true stress–strain curves of the studied lead-free solders at temperatures ranging from 25°C to 110°C and constant strain rate of $1.2 \times 10^{-2}$ $s^{-1}$. It is clear that stress levels of all solders decrease with increasing temperature. High temperature induces lead-free solder softening, but in contrast low temperature contributes to hardening of this lead-free solder. In view of the change of stress–strain curves, it can be determined that mechanical properties of solder alloys showed strong temperature dependence and sensitivity. As

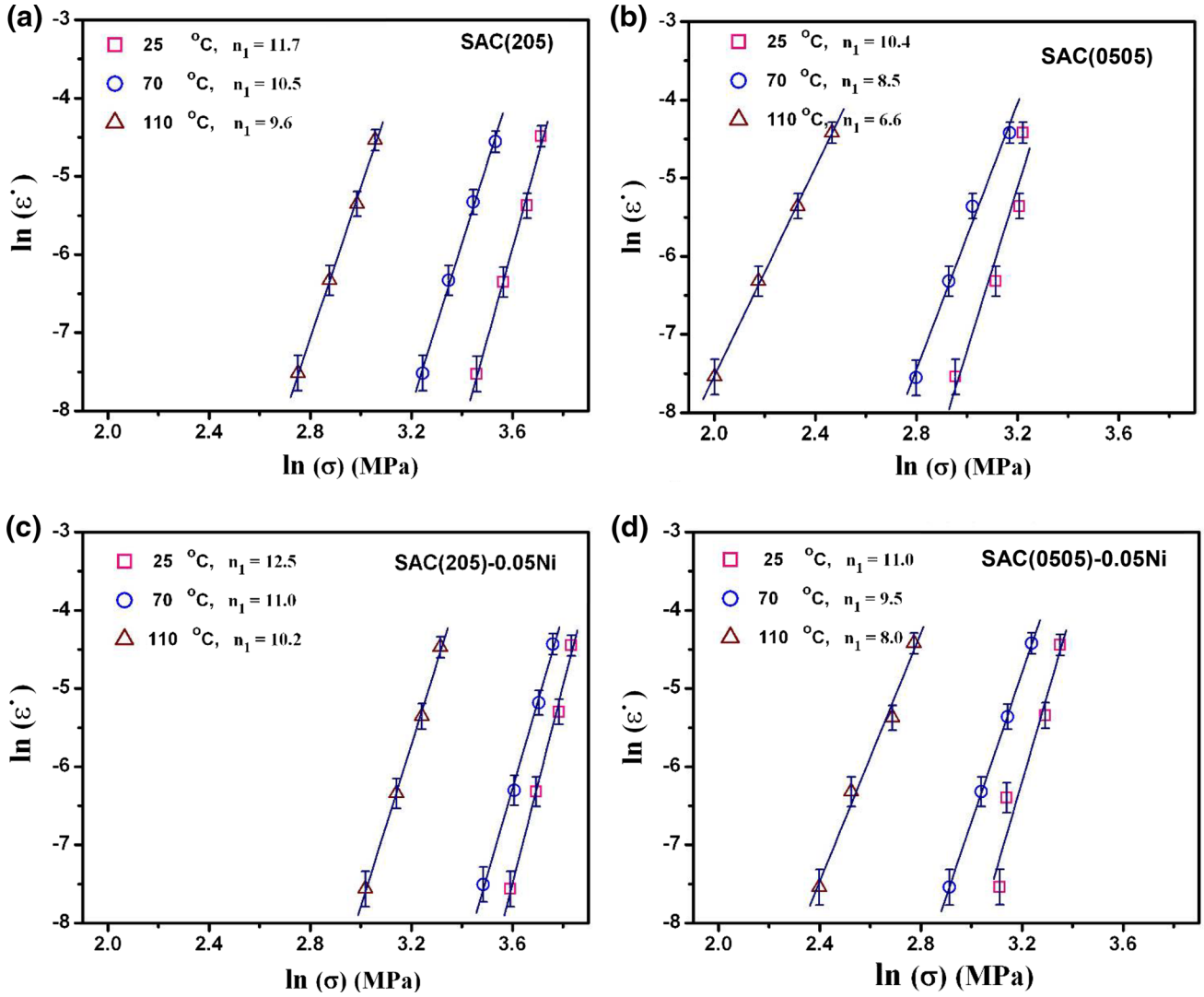


Fig. 10. The relationship between ln ($\dot{\varepsilon}$) versus ln ($\sigma$) at $T$ = 25°C, 70°C and 110°C for (a) SAC (205), (b) SAC (0505), (c) SAC (205)-0.05Ni and (d) SAC (0505)-0.05Ni solder alloys.

shown in Fig. 8, when the testing temperature ascended to 110°C, UTS and YS are much lower than those at the room temperature of 25°C, whereas, the ductility as measured by percent elongation, has decreased and increased with prevailing inconsistent behaviors for solder alloys. Several possible explanations exist for sensitivity of ductility to testing temperatures. These include compositional and heat treatment effects on the matrix phase and IMC chemistries, impurity segregation to interfaces, the nature of the interface formed between the IMCs and the matrix, and the growth rate and stability of the soft and hard IMCs in the alloy matrix.[26]

## Stress Exponent and Activation Energy

In the present investigation, the mechanical deformation mechanism can be determined by calculating values of the characteristic parameters of the stress exponent ($n$) and activation energy ($Q$) according to the following equation[17,27]:

$$\dot{\varepsilon} = A[\sinh(\alpha\sigma)]^n e^{-Q/RT}, \quad (1)$$

where $\dot{\varepsilon}$ is the strain rate, $A$ is a constant, $\alpha$ is a temperature-independent material constant, $\sigma$ is the steady flow stress, $n$ is the stress exponent, $R$ is the gas constant, $T$ is the absolute temperature, $n$ is the stress exponent, and $Q$ is the activation energy for deformation.

The value of $\alpha$ represents the stress reciprocal at which the material deformation changes from power to exponential stress dependence. Therefore, Eq. 1 can be written for low stress level (power law) and high stress level (exponential law) as in Eqs. 2 and 3, respectively, as described elsewhere.[28]

$$\dot{\varepsilon} = A_1\sigma^{n_1}, \quad (2)$$

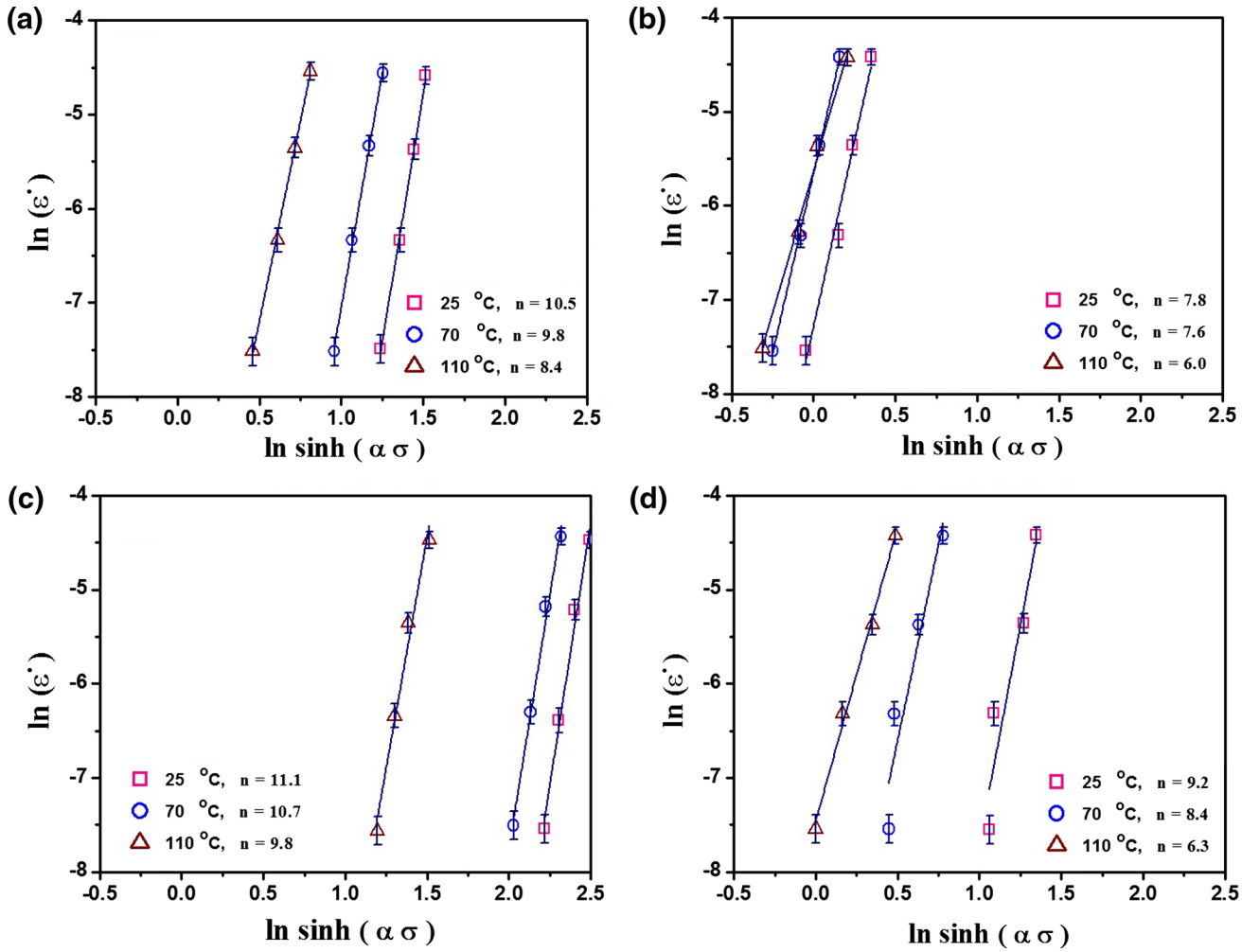


Fig. 11. The relation between ln ($\dot{\varepsilon}$) versus ln [sinh ($\alpha\ \sigma$)] for determination stress exponent ($n$) values at $T = 25$, $T = 70$ and $T = 110$°C for (a) SAC (205), (b) SAC (0505), (c) SAC (205)-0.05Ni and (d) SAC (0505)-0.05Ni solder alloys.

**Table II. The activation energy ($Q$), stress exponent ($n$) and parameter ($\alpha$) values for the examined alloys**

| | | $\alpha$ (MPa$^{-1}$) | | | $n$ | | |
|---|---|---|---|---|---|---|---|
| **Alloy** | **$Q$ (kJ/mol)** | **25°C** | **70°C** | **110°C** | **25°C** | **70°C** | **110°C** |
| SAC (205) | 78.9 | 0.04701 | 0.06000 | 0.07500 | 10.5 | 9.8 | 8.4 |
| SAC (0505) | 53.1 | 0.04423 | 0.05765 | 0.09394 | 7.8 | 7.6 | 6.0 |
| SAC (205)-0.05Ni | 93.6 | 0.05120 | 0.07818 | 0.09020 | 11.1 | 10.7 | 9.8 |
| SAC (0505)-0.05Ni | 72.2 | 0.04727 | 0.06000 | 0.08000 | 9.2 | 8.4 | 6.3 |

$$\dot{\varepsilon} = A_2 e^{\beta\sigma}, \tag{3}$$

where

$$\alpha = \frac{\beta}{n_1}, \tag{4}$$

In the above expressions, the constant $\beta$ is the average slope of the lines $\sigma - \ln \dot{\varepsilon}$ (Fig. 9) and the constant $n_1$ is the average slope of the lines $\ln \sigma - \ln \dot{\varepsilon}$ (Fig. 10). The stress exponent is given by

$$n = \left[\frac{\partial \ln \dot{\varepsilon}}{\partial \ln[\sinh(\alpha\sigma)]}\right]_T, \tag{5}$$

Moreover, the activation energy is obtained from the following expression:

$$Q = R\left[\frac{\partial \ln \dot{\varepsilon}}{\partial \ln\ [\sinh(\alpha\sigma)]}\right]_T \left[\frac{\partial \ln[\sinh(\alpha\sigma)]}{\partial(1/T)}\right]_{\dot{\varepsilon}}. \tag{6}$$

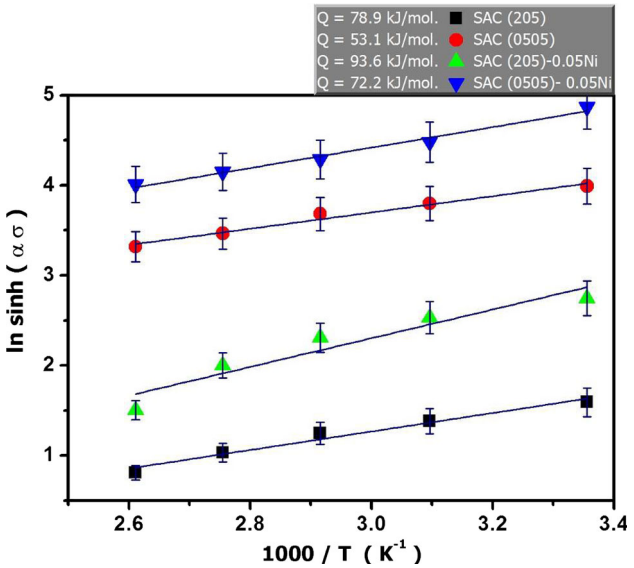


Fig. 12. The relationship between ln sinh ($\alpha\sigma$) versus 1000/T of SAC (205), SAC (0505), SAC (205)-0.05Ni and SAC (0505)-0.05Ni alloys at $\dot{\varepsilon} = 1.2 \times 10^{-2}\ s^{-1}$ for determination activation energy ($Q$) values.

Based on the results shown in Fig. 11, the $n$ values in the temperature range of 25–110°C were estimated to be in the ranges of 10.5–8.4, 7.8–6.0, 11.1–9.8 and 9.2–6.3 for SAC (205), SAC (0505), SAC (205)-0.05Ni and SAC(0505)-0.05Ni alloys, respectively. The temperature dependence of the stress exponent is tabulated in Table II. It is clear that the stress exponent, n, increases with decreasing temperature for all the Pb-free solders, which means that the precipitation-strengthening effect is greater at lower temperature[29] and the instability of the material microstructure at high temperatures[30] for all solder alloys. Comparing the four solder alloys shows that the $n$ values increases with the increment of the Ag content and/or Ni addition. The higher the stress exponent values, the better the strengthening effect of the second phases in matrix Sn. Hence, the large $n$ values observed in SAC (205)-0.05Ni at all tested temperatures are due to the formation of multiple Cu-Ni-Sn intermetallic strengthening phases.[31] In general, diffusional creep is associated with $n$ values around 1, grain boundary sliding leads to $n$ values close to 2 and the dislocation climb is responsible for $n$ values in the 4–6 range. However, the relatively high $n$ values of 8–10 imply that the operative creep mechanism in alloys is dislocation creep.[32]

The activation energy (Q) is determined from plots of ln [sinh ($\alpha\sigma$)] versus (1000/$T$) at constant $\dot{\varepsilon} = 1.2 \times 10^{-2}\,s^{-1}$, as shown in Fig. 12. As demonstrated in Table II, the $Q$ values are 78.9 kJ/mol, 53.1 kJ/mol, 93.6 kJ/mol and 72.2 kJ/mol for SAC (205), SAC (0505), SAC (205)-0.05Ni and SAC (0505)-0.05Ni alloys, respectively. Clearly, the above results indicate that the activation energy of SAC(205)-0.05Ni solder is higher than that of the other solders. Since the Q values for SAC (205), SAC (0505) and SAC (0505)-0.05Ni alloys are lower than the activation energy for the lattice self-diffusion of tin (102 kJ/mol),[33] the activation energies for these solders are relatively close to that for the pipe diffusion of tin. These Q values are close to the 48 kJ/mol and 68 kJ/mol reported for Sn-3.5Ag-0.5Cu-Ni-Ge and Sn-3.0Ag-0.5Cu, respectively.[34] Conversely, the $Q$ value for SAC (205)-0.05Ni is close to the activation energy for lattice self-diffusion of tin (100–130 kJ/mol).[33] This means that increasing Ag content and Ni addition can result in a transition in the controlling tensile mechanism from dislocation-climb-controlled by pipe diffusion to lattice-diffusion-controlled climb of edge dislocation. This transition in the controlling mechanism is likely due to the presence of the fine IMCs in the $\beta$-Sn matrix.

## CONCLUSIONS

Based on the investigations described in the present work, several conclusions may be offered regarding a comparative evaluation of microstructural and mechanical deformation behavior of SAC solders containing 0.05Ni:

(1) Adding 0.05Ni element into SAC solders generated mainly small rod-shaped $(Cu,Ni)_6Sn_5$ IMCs inside the $\beta$-Sn phase. In addition, increasing Ag content affects the size and shapes of IMCs precipitate.
(2) A significant improvement was observed in the mechanical properties of SAC solders with increasing Ag content and Ni addition. Hence, the Sn-2.0Ag-0.5Cu-0.5Ni solder showed the highest tensile strength due to the formation of $(Cu,Ni)_6Sn_5$ IMCs.
(3) The activation energies of lead-free solders were investigated to be 78.9 kJ/mol for SAC (205), 53.1 kJ/mol for SAC (0505), 93.6 kJ/mol for SAC (205)-0.05Ni and 72.2 kJ/mol for SAC (0505)-0.05Ni.

Overall, adding a trace amount of Ni element and increasing Ag content can improve the properties of SAC solders. Thus, the effect of Ag content and element addition on the properties of solder should be comprehensively considered.

## REFERENCES

1. Y.A. Su, L.B. Tan, T.Y. Tee, and V.B.C. Tan, *Microelectron. Reliab.* 50, 564 (2010).
2. S.H. Wang, T.S. Chin, C.F. Yang, S.W. Chen, and C.T. Chuang, *J. Alloys Compd.* 497, 428 (2010).
3. H. Jiang, K. Moon, and C.P. Wong, *Microelectron. Reliab.* 53, 1968 (2013).
4. H. Ye, S. Xue, J. Luo, and Y. Li, *Mater. Des.* 46, 816 (2013).
5. K.C. Otiaba, R.S. Bhatti, N.N. Ekere, S. Mallik, and M. Ekpu, *Eng. Fail. Anal.* 28, 192 (2013).
6. V.L. Niranjani, B.S.S. Chandra Rao, Vajinder Singh, and S.V. Kamat, *Mater. Sci. Eng. A* 529, 257 (2011).
7. S. Chantaramanee, S. Wisutmethangoon, L. Sikong, and T. Plookphol, *J. Mater. Sci.: Mater. Electron.* 24, 3707 (2013).
8. D. Li, C. Liu, and P.P. Conway, *Mater. Sci. Eng. A* 391, 95 (2005).

9. Y.C. Chan and D. Yang, *Prog. Mater. Sci.* 55, 428 (2010).
10. H. Ma and T.K. Lee, *IEEE Trans. Compon. Packag.* 3, 71 (2013).
11. D.A. Shnawah, M.F.M. Sabri, I.A. Badruddin, S.B.M. Said, T. Ariga, and F.X. Che, *J. Electron. Mater.* 42, 470 (2013).
12. David B. Witkin, *Mater. Sci. Eng. A* 532, 212 (2012).
13. R. Pandher and R. Healey, *Proceedings of the 58th Electronic Components and Technology Conference*, *IEEE* (Lake Buena Vista, FL, 2008), p. 2018.
14. U.S. Mohanty and K.L. Lin, *J. Electron. Mater.* 42, 628 (2013).
15. W. Dong, Y. Shi, Y. Lei, Z. Xia, and F. Guo, *J. Mater. Sci.: Mater. Electron.* 20, 1008 (2009).
16. F. Cheng, H. Nishikawa, and T. Takemoto, *J. Mater. Sci.* 43, 3643 (2008).
17. A.A. El-Daly, A.E. Hammad, A. Fawzy, and D.A. Nasrallh, *Mater. Des.* 43, 40 (2013).
18. D. Suh, D.W. Kim, P. Liu, H. Kim, J.A. Weninger, and C.M. Kumar, et al., *Mater. Sci. Eng. A* 460–461, 595 (2007).
19. F.X. Che, W.H. Zhu, S.W. Poh Edith, X.W. Zhang, and X.R. Zhang, *J. Alloys Compd.* 507, 215 (2010).
20. T. Ventura, S. Terzi, M. Rappaz, and A.K. Dahle, *Acta Mater.* 59, 1651 (2011).
21. D.-S. Jiang, Y.-P. Wang, and C.S. Hsiao, *Proceedings of the 8th Electronics Packaging Technology Conference*, *IEEE* (Singapore, 2007), p. 385.
22. A.A. El-Daly and A.E. Hammad, *J. Alloys Compd.* 509, 8554 (2011).
23. G. Montesperelli, M. Rapone, F. Nanni, P. Travaglia, P. Riani, and R. Marazza, et al., *Mater. Corros.* 59, 662 (2008).
24. H.Y. Song, Q.S. Zhu, Z.G. Wang, J.K. Shang, and M. Lu, *Mater. Sci. Eng. A* 527, 1343 (2010).
25. G.Y. Li, B.L. Chen, X.Q. Shi, S.C.K. Wong, and Z.F. Wang, *Thin Solid Films* 504, 421 (2006).
26. A.A. El-Daly, A. Fawzy, A.Z. Mohamad, and A.M. El-Taher, *J. Alloys Compd.* 509, 4574 (2011).
27. J. Zhang, B. Chen, and B. Zhang, *Mater. Des.* 34, 15 (2012).
28. V. Senthilkumar, A. Balaji, and R. Narayanasamy, *Mater. Des.* 37, 102 (2012).
29. M.L. Huang, C.M.L. Wu, and L. Wang, *J. Electron. Mater.* 34, 1373 (2005).
30. S. Alibabaie and R. Mahmudi, *Mater. Des.* 39, 397 (2012).
31. C.M.L. Wu, D.Q. Yu, C.M.T. Law, and L. Wang, *Mater. Sci. Eng. R* 44, 1 (2004).
32. R. Mahmudi, A.R. Geranmayeh, H. Khanbareh, and N. Jahangiri, *Mater. Des.* 30, 574 (2009).
33. I. Shohji, T. Yoshida, T. Takahashi, and S. Hioki, *Mater. Sci. Eng. A* 366, 50 (2004).
34. N. Hidaka, H. Watanabe, and M. Yoshiba, *J. Electron. Mater.* 38, 670 (2009).